

A scalable and robust preconditioner for high-order FEM based on the fast diagonalization method

Pablo D. Brubeck^a, Patrick E. Farrell^a

^a*University of Oxford, Mathematical Institute*

Abstract

Pavarino proved that the additive Schwarz method with vertex patches and a low-order coarse space gives a p -robust solver for symmetric and coercive problems [32]. However, for very high polynomial degree it is not feasible to assemble or factorize the matrices for each patch. In this work we introduce a direct solver for separable patch problems that scales to very high polynomial degree on tensor product cells. The solver constructs a tensor product basis that diagonalizes the blocks in the stiffness matrix for the internal degrees of freedom of each individual cell. As a result, the non-zero structure of the cell matrices is that of the graph connecting internal degrees of freedom to their projection onto the facets. In the new basis, the patch problem is as sparse as a low-order finite difference discretization, while having a sparser Cholesky factorization. We can thus afford to assemble and factorize the matrices for the vertex-patch problems, even for very high polynomial degree. In the non-separable case, the method can be applied as a preconditioner by approximating the problem with a separable surrogate.

1. Introduction

For problems with smooth solutions, high-order finite element methods have very good convergence properties, and in some cases they do not exhibit locking phenomena found in low-order methods. Moreover, due to data-locality and high arithmetic intensity, high-order methods are better suited to make efficient use of modern parallel hardware architectures. Unfortunately, the conditioning of the stiffness matrix is severely affected by the polynomial degree of the approximation. In order to obtain practical iterative solvers, we require good preconditioners.

Optimal solvers are often obtained from a multiplicative multigrid V-cycle where the smoother consists of a domain decomposition method, such as additive Schwarz with a particular space decomposition. The multigrid algorithm is then accelerated by a Krylov subspace method, such as preconditioned conjugate gradients (PCG). The choice of space decomposition in the relaxation is crucial for robustness with respect to the cell size h , the polynomial degree p , and parameters in the equation.

Email addresses: brubeckmarti@maths.ox.ac.uk (Pablo D. Brubeck),
patrick.farrell@maths.ox.ac.uk (Patrick E. Farrell)

One of the cheapest relaxations, with $\mathcal{O}(p^d)$ computational cost, is diagonal scaling, also known as point-Jacobi. The diagonally preconditioned Laplacian has a condition number of $\mathcal{O}(p^{2d-2})$ [28]. This implies that the number of PCG iterations, and therefore the number of residual evaluations, is $\mathcal{O}(p^{d-1})$. In order to minimize the time to solution, it is reasonable to consider more expensive relaxation methods that converge in fewer iterations. Ideally, we wish to balance the cost of applying the relaxation with that of updating the residual. On tensor product elements, the latter operation can be done quickly in $\mathcal{O}(p^{d+1})$ operations via the sum-factorization. Sum-factorization breaks down the residual evaluation into products of one dimensional operators and diagonal scalings [30].

In 1993, Pavarino proved that the additive Schwarz method with a vertex-centered space decomposition and an additive coarse space of lowest-order ($p = 1$) gives a robust solver with respect to h and p for symmetric and coercive problems [32]. This type of space decomposition is often referred to as generous overlap and is illustrated in Figure 1.

The most straightforward implementation of a vertex-patch solver involves the assembly and direct factorization of the $\mathcal{O}(p^d) \times \mathcal{O}(p^d)$ patch matrices (which are dense for Lagrange shape functions). This becomes prohibitively expensive at very high polynomial degrees, with the Cholesky factorization of such a matrix requiring $\mathcal{O}(p^{3d})$ operations. However, there exist bases for which the element matrices are sparse on affine cells, such as the hierarchical Lobatto shape functions [43]. In this basis, the stiffness matrix has a 5-point stencil in 2D, and a much larger 13-point stencil in 3D.

Efficient relaxation methods that are p -robust may arise from the discretization of an auxiliary problem for which fast inversion techniques are available. For a more general approach to auxiliary space techniques, we refer to the work of Xu [46]. In our context, the underlying PDE and the domain can be replaced by those of a problem which is solvable by the method of separation of variables. The fast diagonalization method (FDM) [26] is a $\mathcal{O}(p^{d+1})$ direct factorization that breaks the problem down into a sequence of one-dimensional subproblems. The FDM can only be applied to separable problems, thus it relies on a tensor product grid discretization of the patch, which is only possible when the cells are laid out in a tensor product grid [45]. When the cells are not Cartesian (not all internal angles are right angles), the method of Witte et al. [45] approximates the whole patch as a single Cartesian domain and converges slowly even when the cells are slightly distorted. On general meshes, the patches may not have this structure, thus the FDM cannot be directly applied on such patches. An example of a vertex-centered patch to which the FDM cannot be applied is shown in Figure 2.

A popular alternative in the literature has been to use cell-centered patches with minimal overlap by including a few layers of degrees of freedom (DOFs) of the neighboring cells [18, 37, 42]. This can be done in such a way that every patch remains structured. This kind of space decomposition is more amenable to fast implementation, but does not give a p -robust solver. If the number of layers is fixed, then the measure of the overlap region will decrease as p is increased. Pavarino also proved that when the overlap is not generous, the rate of convergence of the additive Schwarz method will depend inversely on the overlap size [33]. To overcome this, Fischer and Lottes [25] applied a hybrid p -multigrid/Schwarz method, in the context of a Poisson problem. They implemented several levels of p -multigrid to overcome the lack of p -robustness of the cell-centered patches with minimal overlap. The use of multiple levels increases the overlap at the

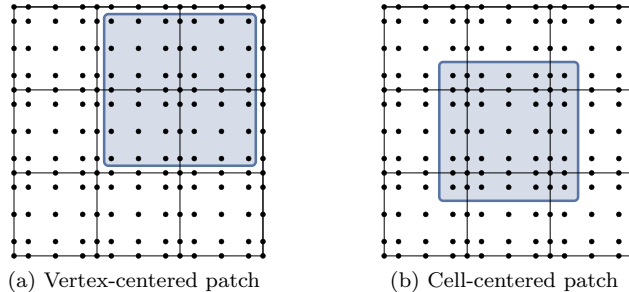


Figure 1: Subdomains for the additive Schwarz method on a regular mesh ($p = 4$). In combination with a low-order coarse grid, the vertex-centered patch gives a p -robust method for symmetric and coercive problems, while the cell-centered patch does not.

coarser levels, but comes at a computational cost. Cell-centered patches without overlap have also been employed for non-symmetric problems [35, 36, 15].

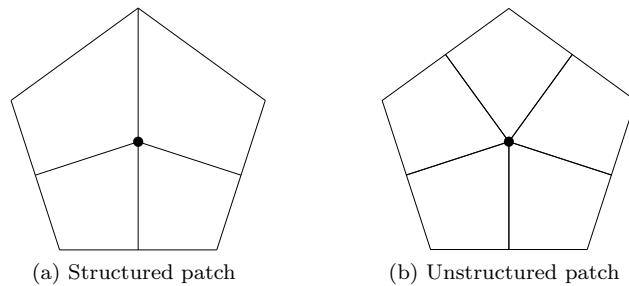


Figure 2: The FDM may be applied as a relaxation only on vertex-centered patches that are structured, i.e. where the cells are laid out in a tensor product grid.

Instead of replacing the vertex-centered patches with cell-centered ones, the alternative FEM-SEM preconditioner discretizes the problem on each vertex-centered patch with $p = 1$ on a GLL grid, a mesh with vertices at the DOFs of the high-order space. The theory behind this guarantees the spectral equivalence between the differential operator discretized on the two spaces [30, 11]. Since low order methods are naturally sparse, this approach is not constrained to Cartesian cells and can deal properly with mixed first derivatives that the FDM cannot handle. For recent developments see [7, 34]. A downside of this approach is that the Cholesky factors of the patch matrices are quite dense, limiting its scalability to very high polynomial degree.

In this work we develop a solver for vertex-centered patches that scales to very high polynomial degree. Our approach does not rely on a particular structure of the patch. In particular, it applies to the patches shown in Figure 2. The key idea is to use the FDM to numerically construct a basis of functions on an interval that diagonalizes the interior blocks of both the stiffness and mass matrices in one dimension. When the problem is assembled with respect to the associated tensor product basis, the resulting stiffness and mass matrices are sparse, in the Cartesian case. In particular, the total number of

non-zeros is the same as that of a low-order finite difference discretization of the Laplacian. Moreover, fill-in in the Cholesky factorization is only introduced for the interface DOFs, resulting in very sparse Cholesky factors. The factorization requires $\mathcal{O}(p^{3(d-1)})$ operations, while forward and back-substitution steps have a cost of $\mathcal{O}(p^{2(d-1)})$ operations that is optimal for $d \in \{2, 3\}$, in contrast with the $\mathcal{O}(p^{3d})$ and $\mathcal{O}(p^{2d})$ costs of the naïve approach. A disadvantage of the approach is that the memory required scales like $\mathcal{O}(p^{2(d-1)})$, instead of the optimal $\mathcal{O}(p^d)$ required for storing the solution. In the non-Cartesian case, we approximate the form with one that is separable in the reference problem. Robustness with respect to h and p should follow from the spectral equivalence between the forms, and numerical experiments indicate that the approach is effective when the cells are moderately deformed.

We demonstrate the effectiveness of our approach by applying it to a $H(\text{div}) \times L^2$ conforming discretization of a mixed formulation of incompressible linear elasticity. We present a sequence of problems of increasing complexity building up to this. In Section 2 we present the standard hp -FEM formulation for the Poisson problem based on a sparse discretization of an auxiliary locally separable PDE that employs the numerically computed FDM basis. In Section 3 we consider the primal formulation of linear elasticity. Although our approach can be applied to patch problems for the individual components of displacement, we explain why it cannot be applied to the coupled vector-valued problem, which is necessary for parameter-robustness in the incompressible regime. We therefore consider a mixed formulation instead. Developing a p -robust solver requires both a p -robust preconditioner and a p -robust discretization, and for the latter we choose a $H(\text{div}) \times L^2$ conforming approach. In Section 5 we extend the method to symmetric interior-penalty discontinuous Galerkin discretizations, required for the displacement block of the mixed problem. In Section 6 we apply our relaxation to the displacement block of the incompressible elasticity system in conjunction with block-preconditioned Krylov methods. We end with conclusions in Section 7.

2. Sparse Poisson solver

We will first describe a solver for the Poisson equation on Cartesian cells, which will subsequently be extended as a preconditioner for more general symmetric coercive problems on non-Cartesian cells.

2.1. Continuous Galerkin formulation

We start from the standard weak formulation of the Poisson equation. Consider a bounded domain $\Omega \subset \mathbb{R}^d$, $d \in \{1, 2, 3\}$, and let $\Gamma_D \subseteq \partial\Omega$ be the part of the boundary where the Dirichlet boundary condition $u|_{\Gamma_D} = u_0$ is prescribed. The problem is to find $u - u_0$ in $V := H_0^1(\Omega) = \{v \in H^1(\Omega), v|_{\Gamma_D} = 0\}$ such that

$$a(v, u) = L(v) \quad \forall v \in V, \quad (2.1)$$

where

$$a(v, u) := \int_{\Omega} \nabla v \cdot \nabla u \, d\mathbf{x}, \quad L(v) := \int_{\Omega} v f \, d\mathbf{x}. \quad (2.2)$$

The standard FEM discretization employs a mesh $\mathcal{T}_h = \{K\}$ of Ω . In this work we consider quadrilateral and hexahedral cells, so that each cell K can be mapped with a

diffeomorphism $F_K : \hat{K} \rightarrow K$ from the reference hypercube $\hat{K} = \hat{\mathcal{I}}^d$, where $\hat{\mathcal{I}} = [-1, 1]$ is the reference interval. The approximate solution $u_h \in V_h$ is sought in the space of piecewise continuous tensor product polynomials on each cell, i.e. $V_h := \mathbb{Q}_p(\Omega) \subset V$. We first define the space of shape functions on \hat{K}

$$\mathbb{Q}_p(\hat{K}) := \bigotimes_{j=1}^d \mathbb{P}_p(\hat{\mathcal{I}}), \quad \mathbb{P}_p(\hat{\mathcal{I}}) := \text{span} \{ \hat{x}^j, 0 \leq j \leq p \}, \quad (2.3)$$

and via composition with F_K^{-1} , we define

$$\mathbb{Q}_p(\Omega) := \left\{ v \in H_0^1(\Omega) : \forall K \in \mathcal{T}_h \exists \hat{v} \in \mathbb{Q}_p(\hat{K}) \text{ s.t. } v|_K = \hat{v} \circ F_K^{-1} \right\}. \quad (2.4)$$

Once we fix a basis $\{\phi_j\}_{j=1}^n$ for V_h , the approximate solution is expanded as $u_h = \sum_{j=1}^n u_j \phi_j$. The resulting $n \times n$ system of linear equations is

$$A \underline{u} = \underline{f}, \quad (2.5)$$

where $[A]_{ij} = a(\phi_i, \phi_j)$ is the stiffness matrix, $\underline{u} = (u_1, \dots, u_n)^\top$ is the vector of coefficients, and $\underline{f} = (L(\phi_1), \dots, L(\phi_n))^\top$ is the load vector.

We recall the standard construction of the basis $\{\phi_j\}$ [21]. The basis is defined in terms of shape functions $\{\hat{\phi}_j\}$ on \hat{K} . Given shape functions $\{\hat{\phi}_j^{1D}\}_{j=0}^p$ for $\mathbb{P}_p(\hat{\mathcal{I}})$, a tensor product basis $\{\hat{\phi}_j\}$ for $\mathbb{Q}_p(\hat{K})$ can be constructed as

$$\hat{\phi}_j(\hat{\mathbf{x}}) = \prod_{k=1}^d \hat{\phi}_{j_k}^{1D}(\hat{x}_k), \quad (2.6)$$

where we have expanded $j = (j_1, \dots, j_d) \in [0, p]^d$ as a multi-index.

The interval shape functions are decomposed into interface and interior modes. The interface modes have non-zero support on either endpoint of $\hat{\mathcal{I}}$, while the interior modes vanish at the boundary of $\hat{\mathcal{I}}$. In multiple dimensions, the shape functions decompose into interior, facet, edge, and vertex modes, depending on how many 1D interface functions are multiplied together. To generate a C^0 basis, we simply match the shape of individual interface modes. Hence, A will be block sparse, since $[A]_{ij} = 0$ when i and j correspond to interior modes supported on different cells.

For the one-dimensional shape functions, one standard choice is the set of Lagrange polynomials on the Gauß–Lobatto–Legendre (GLL) nodes $\{\hat{\xi}_i\}_{i=0}^p \subset [-1, 1]$. These nodes are the roots of $(1 - \hat{\xi}^2)P_p'(\hat{\xi})$, where $P_k(\hat{\xi})$ is the Legendre polynomial of degree k . The Lagrange polynomials $\{\ell_j(\hat{x})\}$ satisfy $\ell_j(\hat{\xi}_i) = \delta_{ij}$ by construction,

$$\ell_j(\hat{x}) = \prod_{k=0, k \neq j}^p \frac{\hat{x} - \hat{\xi}_k}{\hat{\xi}_j - \hat{\xi}_k}, \quad j = 0, \dots, p. \quad (2.7)$$

Another useful basis is formed by the hierarchical Lobatto shape functions $\{l_j\}$, which are constructed by augmenting the so-called bubble functions (integrated Legendre polynomials) with linear nodal functions.

$$l_j(\hat{x}) = \begin{cases} (1 - \hat{x})/2 & \text{for } j = 0, \\ (1 + \hat{x})/2 & \text{for } j = p, \\ \int_0^{\hat{x}} P_j(z) dz & \text{for } j = 1, \dots, p-1. \end{cases} \quad (2.8)$$

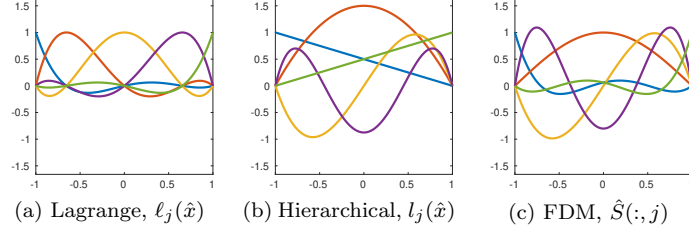


Figure 3: Plots for the one-dimensional shape functions ($p = 4$).

The assembly of the stiffness matrix A is described as follows. On each cell $K \in \mathcal{T}_h$ we define the cell stiffness matrix $A^K \in \mathbb{R}^{(p+1)^d \times (p+1)^d}$ in terms of the basis functions $\{\phi_j^K\}$ that are supported on K , which are obtained from the reference shape functions $\{\hat{\phi}_j\}$ via $\phi_j^K = \hat{\phi}_j \circ F_K^{-1}$. Then, the cell stiffness matrices are

$$[A^K]_{ij} = \int_K \nabla \phi_i^K \cdot \nabla \phi_j^K \, dx. \quad (2.9)$$

The global stiffness matrix is then assembled via direct stiffness summation:

$$A = \sum_{K \in \mathcal{T}_h} R_K^\top A^K R_K, \quad (2.10)$$

where $R_K \in \mathbb{R}^{(p+1)^d \times n}$ is the Boolean restriction matrix from the global DOFs to those local to cell K .

2.2. Tensor product structure on Cartesian meshes

If $d = 1$ and F_K is an affine mapping, then the cell stiffness matrices are

$$[A^K]_{ij} = \frac{1}{L^K} \int_{\hat{\mathcal{I}}} \hat{\phi}_i' \hat{\phi}_j' \, d\hat{x} = \frac{1}{L^K} [\hat{A}]_{ij}. \quad (2.11)$$

Here $\hat{A} \in \mathbb{R}^{(p+1) \times (p+1)}$ is the one-dimensional reference stiffness matrix, and $L^K = |K|/|\hat{\mathcal{I}}|$, where $|K|$ denotes the measure of the cell K .

For $d = \{2, 3\}$, we will first consider the case where Ω can be tessellated with a mesh \mathcal{T}_h consisting of Cartesian cells, i.e. the cells are rectangular quadrilaterals or hexahedra (all internal angles are right angles). In this idealized setting, the cell stiffness matrices are separable in the reference coordinates

$$A^K = \begin{cases} \mu_1^K \hat{B} \otimes \hat{A} + \mu_2^K \hat{A} \otimes \hat{B} & \text{if } d = 2, \\ \mu_1^K \hat{B} \otimes \hat{B} \otimes \hat{A} + \mu_2^K \hat{B} \otimes \hat{A} \otimes \hat{B} + \mu_3^K \hat{A} \otimes \hat{B} \otimes \hat{B} & \text{if } d = 3, \end{cases} \quad (2.12)$$

where

$$[\hat{B}]_{ij} = \int_{\hat{\mathcal{I}}} \hat{\phi}_i \hat{\phi}_j \, d\hat{x}, \quad (2.13)$$

is the one-dimensional reference mass matrix, $\mu_j^K = (L_j^K)^{-2} \prod_{i=1}^d L_i^K$, and L_j^K is the length of K along the j -th axis divided by $|\hat{\mathcal{I}}|$. The symbol \otimes denotes the standard

Kronecker product, which for matrices $A \in \mathbb{R}^{m \times n}$, $B \in \mathbb{R}^{r \times s}$, is defined as the block matrix

$$A \otimes B = \begin{bmatrix} a_{11}B & \cdots & a_{1n}B \\ \vdots & \ddots & \vdots \\ a_{m1}B & \cdots & a_{mn}B \end{bmatrix} \in \mathbb{R}^{rm \times sn}. \quad (2.14)$$

It follows that if A and B are sparse, then $A \otimes B$ is also sparse.

For the Lagrange nodal basis $\{\ell_j\}$, both \hat{A} and \hat{B} are dense, but these are sparse in the hierarchical Lobatto basis $\{l_j\}$. This is illustrated in Figure 4. On affine cells, the Lobatto basis yields a sparse stiffness matrix. The bubble functions $\{l_j\}_{j=1}^{p-1}$, satisfy $l'_j(\hat{x}) = P_j(\hat{x})$, and due to the orthogonality of the Legendre polynomials, the interior block of \hat{A} is diagonal. The only off-diagonal non-zeros in \hat{A} are due to the coupling between the interface modes l_0, l_p . Nevertheless, in order for this sparsity to propagate to higher dimensions, we would additionally wish that \hat{B} is also as sparse as possible. This is not quite the case for $\{l_j\}$, as \hat{B} has two interior blocks with tri-diagonal structure, in the ordering which groups the odd modes first and then the even modes. Therefore, on a typical row, A will have the structure of the 5-point stencil for $d = 2$ and that of a 13-point stencil for $d = 3$.

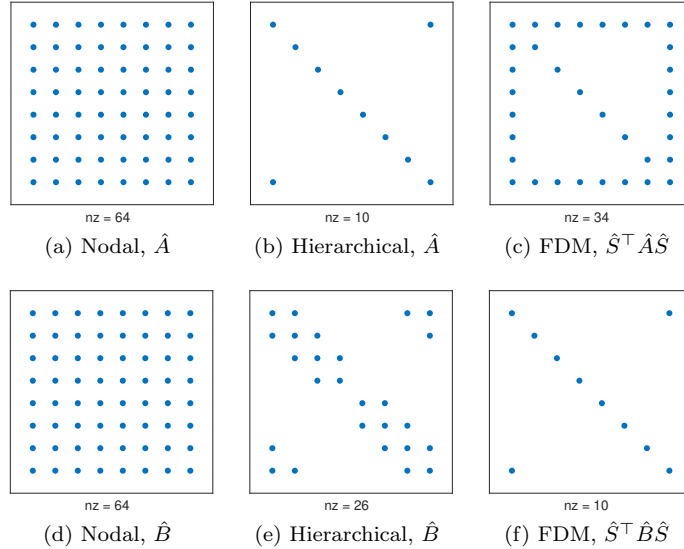


Figure 4: Non-zero structure of \hat{A}, \hat{B} ($p = 7$).

2.3. The fast diagonalization method

The fast diagonalization method (FDM) [26] is a direct factorization technique for structured matrices such as that defined in (2.12). This method reduces the computation into a sequence of eigenvalue problems on the interval in a similar fashion as the method of separation of variables. To illustrate the FDM, we consider solving a problem on the interior of a single cell. We decompose the vector of coefficients as $\underline{u} = \underline{u}_I + \underline{u}_\Gamma$, and

suppose that the entries of \underline{u}_Γ corresponding to the interface DOFs are specified. Let $R_I^K \in \mathbb{R}^{(p-1)^d \times n}$ be the Boolean restriction matrix onto the interior DOFs of K . The local correction $\underline{u}_I^K = R_I^K \underline{u}_I$, is decoupled from the other cells, and thus may be solved in parallel via $A_{II}^K \underline{u}_I^K = R_I^K (b - A \underline{u}_\Gamma)$, where $A_{II}^K = R_I^K A R_I^{K\top}$.

To solve the local problems in the Cartesian case, we may first solve the generalized eigenvalue problem on the interior of the reference interval

$$\hat{A}_{II} \hat{S}_{II} = \hat{B}_{II} \hat{S}_{II} \hat{\Lambda}_{II}, \quad (2.15)$$

in conjunction with the normalization condition $\hat{S}_{II}^\top \hat{B}_{II} \hat{S}_{II} = \mathbf{1}$. Here $\hat{A}_{II}, \hat{B}_{II} \in \mathbb{R}^{(p-1) \times (p-1)}$ are the interior blocks of \hat{A} and \hat{B} respectively, $\hat{\Lambda}_{II} \in \mathbb{R}^{(p-1) \times (p-1)}$ is the diagonal matrix of eigenvalues, and $\hat{S}_{II} \in \mathbb{R}^{(p-1) \times (p-1)}$ is the matrix of eigenvectors. The generalized eigenproblem (2.15) may be equivalently rewritten as

$$\hat{S}_{II}^\top \hat{A}_{II} \hat{S}_{II} = \hat{\Lambda}_{II}, \quad \hat{S}_{II}^\top \hat{B}_{II} \hat{S}_{II} = \mathbf{1}. \quad (2.16)$$

The corresponding continuous problem is to find $s_j(\hat{x})$ and $\lambda_j, j = 1, \dots, p-1$, such that

$$\int_{\mathcal{I}} s'_i(\hat{x}) s'_j(\hat{x}) \, d\hat{x} = \lambda_j \delta_{ij}, \quad \int_{\mathcal{I}} s_i(\hat{x}) s_j(\hat{x}) \, d\hat{x} = \delta_{ij}, \quad s_j(\pm 1) = 0, \quad (2.17)$$

with solution $s_j(\hat{x}) = \sin(j\pi(1 + \hat{x})/2)$, $\lambda_j = j^2 \pi^2/4$. Thus, \hat{S}_{II} approximates a discrete sine transform on the GLL nodes.

If A^K is given by (2.12), then we have the following diagonal factorization for the inverse

$$(A_{II}^K)^{-1} = \bigotimes_{k=1}^d \hat{S}_{II} (\Lambda_{II}^K)^{-1} \bigotimes_{k=1}^d \hat{S}_{II}^\top, \quad (2.18)$$

where

$$\Lambda_{II}^K = \begin{cases} \mu_1^K \mathbf{1} \otimes \hat{\Lambda}_{II} + \mu_2^K \hat{\Lambda}_{II} \otimes \mathbf{1} & \text{if } d = 2, \\ \mu_1^K \mathbf{1} \otimes \mathbf{1} \otimes \hat{\Lambda}_{II} + \mu_2^K \mathbf{1} \otimes \hat{\Lambda}_{II} \otimes \mathbf{1} + \mu_3^K \hat{\Lambda}_{II} \otimes \mathbf{1} \otimes \mathbf{1} & \text{if } d = 3. \end{cases} \quad (2.19)$$

Therefore, the solution of a system $A_{II}^K \underline{u}_I^K = \underline{r}_I^K$ can be obtained with $\mathcal{O}(p^{d+1})$ computational work.

The main limitation of this approach is that it does not generalize to terms that contain first derivatives. Mixed first derivative terms are very common in symmetric coercive problems, for instance, when the cells have non-orthotropic deformations, or for vector-valued problems that mix first derivatives of distinct vector components, such as $\nabla \cdot \mathbf{u} \nabla \cdot \mathbf{v}$ or $\nabla \times \mathbf{u} \cdot \nabla \times \mathbf{v}$.

2.4. Sparse stiffness matrix via the FDM

We propose to use the eigenvectors of the FDM to define one-dimensional shape functions for which the corresponding tensor product basis yields a sparse stiffness matrix. Numerically, it is most convenient to define the coefficients of the new basis with respect to the nodal or hierarchical basis. One might choose transform the whole problem upfront, but we decide to keep the nodal shape functions and transform back and forth from the nodal space to the modal FDM space every time we apply the solver. This is

because we might also wish to compute other quantities from the solution, in particular for nonlinear problems.

The interior shape functions are chosen such that they simultaneously diagonalize the interior blocks of \hat{A} and \hat{B} , while vanishing on the interface. For the facet functions, we use nodal interface functions, with support extended into the interior in such a way that \hat{B} becomes as sparse as possible in the new basis. The coefficients of the 1D basis are given as the columns of the $(p+1) \times (p+1)$ matrix

$$\hat{S} = \begin{bmatrix} \hat{S}_{II} & \hat{S}_{I\Gamma} \\ 0 & \mathbf{1} \end{bmatrix}, \quad (2.20)$$

where the rows and columns are ordered such that the interior DOFs are followed by the interface DOFs, and

$$\hat{S}_{I\Gamma} = -\hat{S}_{II}\hat{S}_{II}^\top\hat{B}_{I\Gamma} \quad (2.21)$$

is chosen such that the (I, Γ) and (Γ, I) -blocks of $\hat{S}^\top\hat{B}\hat{S}$ vanish. As it is evident from Figure 4, $\hat{S}^\top\hat{A}\hat{S}$ will not be as sparse as \hat{A} discretized with the hierarchical Lobatto shape functions. But the advantage is that $\hat{S}^\top\hat{B}\hat{S}$ has maximal sparsity, which is crucial in higher dimensions.

It would then follow that the stiffness matrix for a cell in this new basis,

$$\tilde{A}^K = \bigotimes_{k=1}^d \hat{S}^\top A^K \bigotimes_{k=1}^d \hat{S}, \quad (2.22)$$

has structured sparsity. Due to the distributive property of the Kronecker product under matrix multiplication, \tilde{A}^K has the same form of (2.12) but with $\hat{S}^\top\hat{A}\hat{S}$ and $\hat{S}^\top\hat{B}\hat{S}$ instead of \hat{A} and \hat{B} . Moreover, if we wish to sparsify the global stiffness matrix A , we can define the global basis

$$S = W^{-1} \sum_{K \in \mathcal{T}_h} R_K^\top \left\{ \bigotimes_{k=1}^d \hat{S} \right\} R_K \quad (2.23)$$

where $W = \sum_{K \in \mathcal{T}_h} R_K^\top R_K = \text{diag}(w_i)$ is the diagonal matrix with the multiplicity of each DOF. Then, the transformed matrix $S^\top A S$ can be assembled via direct stiffness summation:

$$\tilde{A} = S^\top A S = \sum_{K \in \mathcal{T}_h} R_K^\top \tilde{A}^K R_K. \quad (2.24)$$

Then, we obtain a solver that can benefit from sparse direct factorization methods or other preconditioners such as additive Schwarz applied to \tilde{A} , since

$$A^{-1} = S \tilde{A}^{-1} S^\top. \quad (2.25)$$

Our approach replaces the diagonal matrix of the traditional FDM with the sparse matrix \tilde{A} , which can be assembled even on 3D meshes with a very large number of cells and for very high degree. This approach removes the requirement of a global tensor product grid while exploiting the separability of the PDE and the local structure of $Q_p(\Omega)$, at the expense of replacing the diagonal factor by a sparse matrix.

2.5. Hybrid p -multigrid/Schwarz method

The solver of Pavarino is fully additive, across both the coarse grid and the vertex patches. In our work we consider a small variation of this, with the solver multiplicative between the two levels while remaining additive among the vertex patches. This improves the convergence at essentially no cost. The method can be interpreted as a hybrid multiplicative two-level $V(1, 1)$ -cycle with the additive Schwarz method [16] with vertex-centered patches as the fine grid relaxation and the lowest-order discretization on the same mesh as the coarse space. In most of our experiments, the sparse matrix for the coarse space is assembled and factorized, but other preconditioners such as geometric or algebraic multigrid may be applied instead. The vertex-centered patch V_j includes the degrees of freedom associated with vertex \mathbf{v}_j of \mathcal{T}_h and all cells, facets, and edges adjacent to \mathbf{v}_j (the topological entities in the *star* of the vertex, to use the terminology of [17]).

Exploiting the basis in which the problem becomes sparse, we may write the multigrid relaxation as

$$P_{\text{smooth}}^{-1} = S \tilde{A}_{\text{ASM}}^{-1} S^\top, \quad (2.26)$$

where

$$\tilde{A}_{\text{ASM}}^{-1} = \sum_{j=1}^J \bar{R}_j^\top \tilde{A}_j^{-1} \bar{R}_j, \quad (2.27)$$

with \bar{R}_j the Boolean restriction matrix onto V_j , and

$$\tilde{A}_j = \bar{R}_j \tilde{A} \bar{R}_j^\top \quad (2.28)$$

are the sparse patch matrices for which we may explicitly compute a Cholesky decomposition. In order to ensure that $\mathbf{1} - \omega P_{\text{smooth}}^{-1} A$ is contractive, we use a damping coefficient $\omega = (\lambda_{\max} + \lambda_{\min})/2$, where the extremal eigenvalues of $P_{\text{smooth}}^{-1} A$ are estimated via the CG-Lanczos procedure [22].

To illustrate the direct solver on the Cartesian vertex-centered patch shown in Figure 1a, we show in Figure 5 the non-zero structure for the transformed stiffness matrix \tilde{A} and its Cholesky factor. The sparsity pattern of the transformed global matrix \tilde{A} connects the interior DOFs to their projections onto the facets, hence a typical interior row of \tilde{A} will have $2d + 1$ non-zeros. For the patch matrix \tilde{A}_j , an interior row will only have $d + 1$ non-zeros, as the patch only includes one facet per dimension on each cell. Moreover, the total number of non-zeros of \tilde{A}_j is the same as that of a low-order finite difference or finite element discretization with the 5-point or 7-point stencil on the same grid.

2.6. Computational complexity

Here we discuss the computational cost of applying the basis transformation and the solution of the patch problem using the Cholesky factorization. Once the factorization has been computed, it may be applied in $\mathcal{O}(p^{2(d-1)})$ cost, which is optimal for $d \in \{2, 3\}$. Unfortunately, the factorization phase is suboptimal, requiring $\mathcal{O}(p^{3(d-1)})$ operations to compute. The memory required to store the Cholesky factor is $\mathcal{O}(p^{2(d-1)})$, which for $d = 3$ is one factor of p higher than that required to store the solution.

In order to maximize the sparsity in the Cholesky factor, it is crucial to reorder the DOFs, such that interior DOFs are followed by the interface DOFs, which are grouped

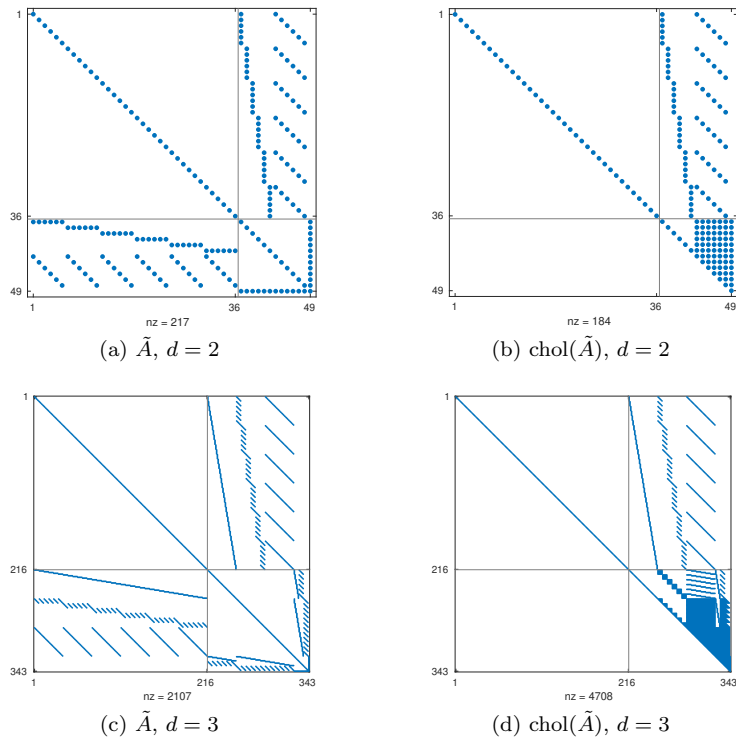


Figure 5: Non-zero structure of the stiffness matrix in the FDM basis $\tilde{A} = S^T A S = L L^T$ and its upper Cholesky factor L^T for the Poisson problem on a Cartesian vertex patch with $p = 4$. Here we have reordered the unknowns with nested dissection in order to achieve fill-in only on the bottom-right block.

into separator planes formed by the facets, edges, and then the vertex. To analyze the complexity of the Cholesky factorization of \tilde{A} on any mesh with all cells Cartesian, we first introduce the block LDL^\top decomposition

$$\tilde{A} = \begin{bmatrix} \tilde{A}_{II} & \tilde{A}_{I\Gamma} \\ \tilde{A}_{\Gamma I} & \tilde{A}_{\Gamma\Gamma} \end{bmatrix} = \begin{bmatrix} \mathbf{1} & 0 \\ \tilde{A}_{\Gamma I} \tilde{A}_{II}^{-1} & \mathbf{1} \end{bmatrix} \begin{bmatrix} \tilde{A}_{II} & 0 \\ 0 & \tilde{\Sigma}_{\Gamma\Gamma} \end{bmatrix} \begin{bmatrix} \mathbf{1} & \tilde{A}_{II}^{-1} \tilde{A}_{I\Gamma} \\ 0 & \mathbf{1} \end{bmatrix}, \quad (2.29)$$

where $\tilde{\Sigma}_{\Gamma\Gamma} = \tilde{A}_{\Gamma\Gamma} - \tilde{A}_{\Gamma I} \tilde{A}_{II}^{-1} \tilde{A}_{I\Gamma}$ is the interface Schur complement. By construction, the top-left block \tilde{A}_{II} is diagonal with positive entries, implying that its Cholesky factor is equal to its square root $\tilde{A}_{II}^{1/2}$, which is well defined. If we decompose \tilde{A}_{II} and $\tilde{\Sigma}_{\Gamma\Gamma}$ in the second matrix on the RHS of (2.29) into their Cholesky factors, and distribute each factor onto the other two matrices, we obtain the Cholesky decomposition of \tilde{A}

$$\tilde{A} = LL^\top = \begin{bmatrix} \tilde{A}_{II}^{1/2} & 0 \\ \tilde{A}_{\Gamma I} \tilde{A}_{II}^{-1/2} & L_\Gamma \end{bmatrix} \begin{bmatrix} \tilde{A}_{II}^{1/2} & \tilde{A}_{II}^{-1/2} \tilde{A}_{I\Gamma} \\ 0 & L_\Gamma^\top \end{bmatrix}, \quad (2.30)$$

where the Schur complement is factorized as $\tilde{\Sigma}_{\Gamma\Gamma} = L_\Gamma L_\Gamma^\top$. Since \tilde{A}_{II} is diagonal, the off-diagonal block $\tilde{A}_{\Gamma I} \tilde{A}_{II}^{-1/2}$ will preserve the non-zero structure of $\tilde{A}_{\Gamma I}$, and similarly for its transpose. Therefore, fill-in is only introduced on the interface block through L_Γ .

Assuming for the worst case that L_Γ^\top is dense, the memory required to store the Cholesky factor is $\mathcal{O}(p^{2(d-1)})$. This represents a significant increase from the traditional FDM, which is kept at the optimal $\mathcal{O}(p^d)$. However, the DOF ordering does lead to some structured sparsity in L_Γ^\top , as can be seen in Figure 5. The top rows of L_Γ^\top correspond to the first group of facets which form a separator plane. There, the fill-in is $\mathcal{O}(p^{d-2})$, while the rest of the separator planes introduce dense $\mathcal{O}(p^{d-1}) \times \mathcal{O}(p^{d-1})$ blocks on the rows below. The fact that L_Γ^\top contains these dense blocks indicates that $\mathcal{O}(p^{3(d-1)})$ operations are required in the factorization phase.

Compared to the FEM-SEM approach, our approach with the FDM basis has a sparser Cholesky factorization. If we consider $d = 2$ and a Cartesian vertex-centered patch, the Cholesky factor of the low-order rediscretization will require $\mathcal{O}(p^2 \log(p^2))$ storage when the DOFs are reordered with nested dissection [19], in contrast with the $\mathcal{O}(p^2)$ storage required by our approach. In Figure 6 we present the ratio of the number of non-zeros in the Cholesky factors of our approach and the FEM-SEM preconditioner for $d \in \{2, 3\}$. The fact that the ratio is always below 1 confirms that our approach is sparser, with a substantial gain at higher degrees.

On the other hand, the forward and back-substitution steps have a computational cost of $\mathcal{O}(p^{2(d-1)})$ operations. For $d = 2$, this is $\mathcal{O}(p^2)$, the same cost of diagonal scaling, therefore the asymptotic cost of the traditional FDM is retained. For $d = 3$, the cost is $\mathcal{O}(p^4)$, which is the same $\mathcal{O}(p^{d+1})$ cost of the traditional FDM involved in the multiplication times S .

We plot in Figure 7 the time taken for FDM basis transformation (applying S and S^\top), Cholesky factorization, and solution via forward and back-substitution, as a function of p . The problem is posed on a vertex patch of 2^d cells, with the Cholesky factorization computed using CHOLMOD [12]. Surprisingly, these results show $\mathcal{O}(p^{d+1})$ scaling for the Cholesky factorization step in $d = 3$. At present we are unable to explain this unexpected speedup.

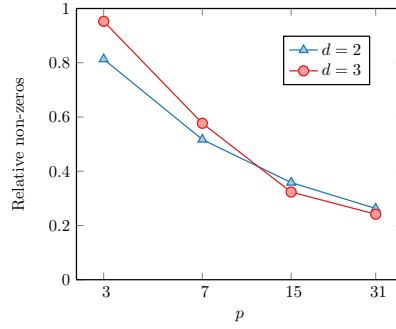
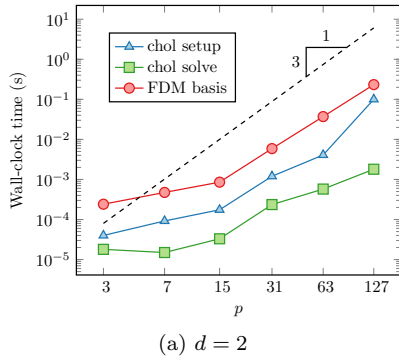
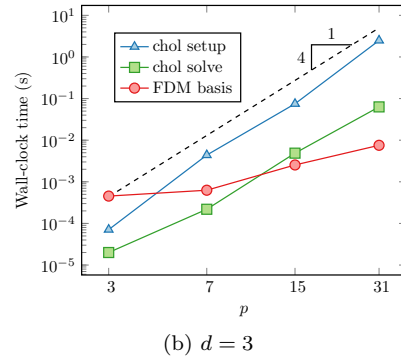


Figure 6: Relative number of non-zero entries in the Cholesky factors of the stiffness matrix with the FDM approach and the FEM-SEM preconditioner, for a Cartesian vertex patch of 2^d cells. The FDM approach is sparser, with substantial gains at higher degrees.



(a) $d = 2$



(b) $d = 3$

Figure 7: Wall-clock runtimes for the Cholesky factorization of \tilde{A} , solution of a linear system and the matrix-vector products with the FDM basis S and its transpose for a Cartesian vertex patch of 2^d cells. For $d = 3$, we observe that the time to factorize scales better than expected, close to the optimal $\mathcal{O}(p^{d+1})$ complexity.

2.7. Extension to non-Cartesian meshes

For arbitrarily deformed cells, the local stiffness matrices A^K cannot be expressed in terms of tensor products of \hat{A} and \hat{B} as in (2.12). Therefore, the basis \hat{S} cannot sparsify A^K . The preconditioning techniques found in [14, 18, 45] introduce an auxiliary Cartesian domain to construct a separable problem for which the FDM is a direct solver. The method described by Fischer [18] constructs a preconditioner by replacing K with its nearest rectangular approximation, whose dimensions are computed as the mean separation between the mapped GLL nodes from opposite facets of K . Witte et al. [45] obtain the lengths from the average arclength of opposite sides of K , but it is not clear how this extends to the 3D case. To the best of our knowledge, no theory underpins these choices.

Our approach to construct the separable surrogate is based on the theory of equivalent operator preconditioning [5]. We work with the variational form $a(\cdot, \cdot)$ in terms of the reference coordinates. We simply discard the mixed derivative terms that prevent separability, and we replace the coefficients with piecewise constants in the reference coordinates¹. We will prove that this choice yields a spectrally equivalent operator.

The bilinear form $a(\cdot, \cdot)$ can be expressed as a sum of cell contributions $a_K(\cdot, \cdot)$ where integration and differentiation are with respect to $\hat{\mathbf{x}}$. The measure $d\mathbf{x}$ is replaced by $|\det(\mathbf{D}F_K)|d\hat{\mathbf{x}}$ and the gradient is computed via the chain rule, since the arguments of the form become functions of $\hat{\mathbf{x}}$ after being composed with F_K . Hence,

$$a(v, u) = \sum_{K \in \mathcal{T}_h} a_K(v, u) = \sum_{K \in \mathcal{T}_h} \int_{\hat{K}} \hat{\nabla} v \circ F_K \cdot \hat{G}^K \hat{\nabla} u \circ F_K \, d\hat{\mathbf{x}}, \quad (2.31)$$

where $\hat{\nabla}$ is the gradient with respect to $\hat{\mathbf{x}}$, and $\hat{G}^K : \hat{K} \rightarrow \mathbb{R}^{d \times d}$ is the inverse metric of the coordinate transformation weighted by the Jacobian determinant,

$$\hat{G}^K = |\det(\mathbf{D}F_K)| \mathbf{D}F_K^{-1} \mathbf{D}F_K^{-\top}. \quad (2.32)$$

This tensor encapsulates all of the geometry-dependent information in the form; it is spatially dependent for generally-deformed elements, and constant in the case of affine transformations. For a separable geometry, \hat{G}^K is diagonal, and thus for a Cartesian cell it is diagonal and constant. To construct an auxiliary problem that is separable by the FDM in the reference coordinates, we replace \hat{G}^K in $a_K(\cdot, \cdot)$ with a constant diagonal approximation $\text{diag}(\mu_j^K)$. Each μ_j^K is given by the cell-wise average of the diagonal entry \hat{G}_{jj}^K ,

$$\mu_j^K := \frac{1}{|\hat{K}|} \int_{\hat{K}} \hat{G}_{jj}^K \, d\hat{\mathbf{x}}, \quad (2.33)$$

where summation over the index j is not implied. As the approximation is local to each cell, it is still possible to assemble a stiffness matrix on meshes where cells are not structured in a tensor product grid.

We now establish the spectral equivalence between the original bilinear form and the auxiliary separable one.

¹Recall that piecewise constant coefficients in the physical coordinates will not yield piecewise constant coefficients in the reference coordinates.

Theorem 1. Let $\hat{\mu}_K := \text{diag}(\mu_j^K)$ be the constant diagonal approximation of \hat{G}^K , and define the auxiliary bilinear form

$$b(v, u) := \sum_{K \in \mathcal{T}_h} b_K(v, u) := \sum_{K \in \mathcal{T}_h} \int_{\hat{K}} \hat{\nabla} v \circ F_K \cdot \hat{\mu}_K \hat{\nabla} u \circ F_K \, d\hat{\mathbf{x}}. \quad (2.34)$$

Then, there exist p -independent constants $c, C > 0$ that depend on \mathcal{T}_h through \hat{G}^K such that

$$c \leq \frac{a(v, v)}{b(v, v)} \leq C \quad \forall v \in V \setminus \{0\}. \quad (2.35)$$

Proof. Let c_K, C_K be lower and upper bounds for the spectrum of the diagonally scaled metric, so that $\sigma(\hat{\mu}_K^{-1/2} \hat{G}^K \hat{\mu}_K^{-1/2}) \in [c_K, C_K]$ for all $\hat{\mathbf{x}} \in \hat{K}$. We claim that

$$c_K \leq \frac{a_K(v, v)}{b_K(v, v)} \leq C_K \quad \forall v \in \{v \in V : v|_K \neq 0\}. \quad (2.36)$$

This result is obtained by first rewriting $a_K(v, v)$ with $\hat{\mu}_K^{1/2} \hat{\mu}_K^{-1/2} \hat{G}^K \hat{\mu}_K^{-1/2} \hat{\mu}_K^{1/2}$ instead of \hat{G}^K , and then replacing $\hat{\mu}_K^{-1/2} \hat{G}^K \hat{\mu}_K^{-1/2}$ with $c_K \mathbf{1}$ or $C_K \mathbf{1}$ to find the lower or upper bounds, respectively. It then follows that

$$c := \min_{K \in \mathcal{T}_h} c_K \leq \frac{a(v, v)}{b(v, v)} \leq \max_{K \in \mathcal{T}_h} C_K =: C \quad \forall v \in V \setminus \{0\}. \quad (2.37)$$

□

Let B be the stiffness matrix associated with the auxiliary form $b(\cdot, \cdot)$. By Theorem 1, the condition number $\kappa(B^{-1}A)$ is bounded by C/c independently of p . Numerical experiments also indicate that $\kappa(B^{-1}A)$ is independent of h under uniform refinements. Now consider a preconditioner P where the auxiliary form $b(\cdot, \cdot)$ is used additively in both the coarse solve and the vertex-centered patches. In this case, Theorem 1 of [32] guarantees that $\kappa(P^{-1}B)$ is bounded from above independently of h and p . Hence we may conclude that $\kappa(P^{-1}A) \leq \kappa(P^{-1}B)\kappa(B^{-1}A)$ is bounded independently of h and p . In practice, we expect that using multiplicative coarse grid correction with the original form $a(\cdot, \cdot)$ can only improve the preconditioner.

To gain useful insight, we consider the case where $d = 2$ and F_K is an affine transformation, that is when K is a parallelogram. Without loss of generality, suppose that one of the sides of K has length $2L_1$ and is aligned with the first reference coordinate axis, and the other side of length $2L_2$ is at an angle θ with respect to the same axis. The Jacobian of the coordinate transformation is

$$DF_K = \begin{bmatrix} L_1 & L_2 \cos \theta \\ 0 & L_2 \sin \theta \end{bmatrix}, \quad (2.38)$$

to which corresponds the Jacobian-weighted inverse metric

$$\hat{G}^K = \frac{1}{L_1 L_2 |\sin \theta|} \begin{bmatrix} L_2^2 & -L_1 L_2 \cos \theta \\ -L_1 L_2 \cos \theta & L_1^2 \end{bmatrix}. \quad (2.39)$$

Since \hat{G}^K is constant, $\hat{\mu}_K$ is simply the diagonal part of \hat{G}^K . The spectrum of the diagonally scaled metric will be independent of L_1 and L_2 , but it will still depend on θ ,

$$\sigma\left(\hat{\mu}_K^{-1/2}\hat{G}^K\hat{\mu}_K^{-1/2}\right) = [1 - |\cos\theta|, 1 + |\cos\theta|]. \quad (2.40)$$

This spectrum is desirable because it is centered at 1 and bounded above for all θ . If we follow the geometric approaches of [18, 45], we would have to choose a rectangle with side lengths $2L_1$ and $2L_2$ as the auxiliary domain. Then, the previous bounds (2.40) would become scaled by $|\sin\theta|^{-1}$. In this case, the spectrum is unbounded from above in the limit $\theta \rightarrow 0$.

2.8. Numerical experiments

The hybrid p -multigrid/Schwarz solver employing the FDM/sparse relaxation is illustrated in Figure 8. To achieve scalability with respect to the mesh parameter h , on the p -coarse problem we employ geometric multigrid with damped point-Jacobi relaxation and a direct Cholesky factorization on the coarsest level. We test the effectiveness of this approach on a hierarchy of meshes obtained by $l \geq 0$ uniform refinements of the base meshes shown in Figure 9.

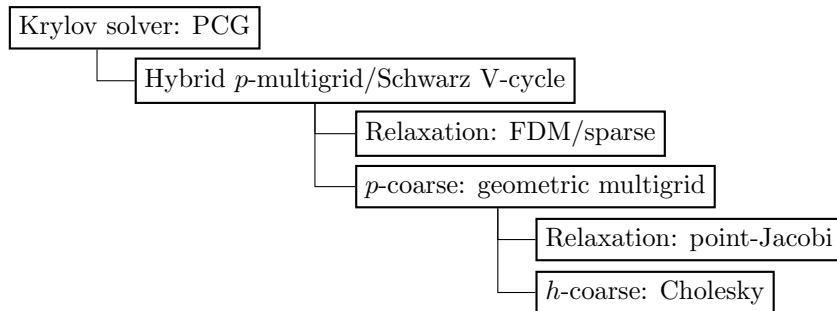


Figure 8: Solver diagram for the Poisson problem.

In Table 1 we present results for the Poisson equation in $\Omega = (0, 1)^d$ discretized on the two hierarchies of Cartesian and unstructured meshes. We impose homogeneous Dirichlet BCs on $\Gamma_D = \partial\Omega$ and a constant forcing $f = 1$. We show the condition number κ estimated by CG-Lanczos and the number of PCG iterations required to reduce the Euclidean norm of the residual by a factor of 10^8 starting from a zero initial guess. The results show almost complete p - and h -robustness in the Cartesian case, and very slow growth of iteration counts in the unstructured case.

We now consider an experiment to test the sharpness of the spectral equivalence bounds derived in the previous section. In Tables 2a and 2b we consider the Poisson equation discretized on a 3×3 parallelogram mesh with an interior angle of θ and sides of unit length. The mesh for $\theta = 2\pi/8$ is shown in Figure 10. For different values of θ and p , we apply the FDM/sparse relaxation without the coarse space. We present the ratio between the extremal eigenvalues of the preconditioned matrix and the bounds for the spectrum of the diagonally scaled metric. The first column corresponds to the unit square. According to our theory, the columns in Table 2a should be bounded from below

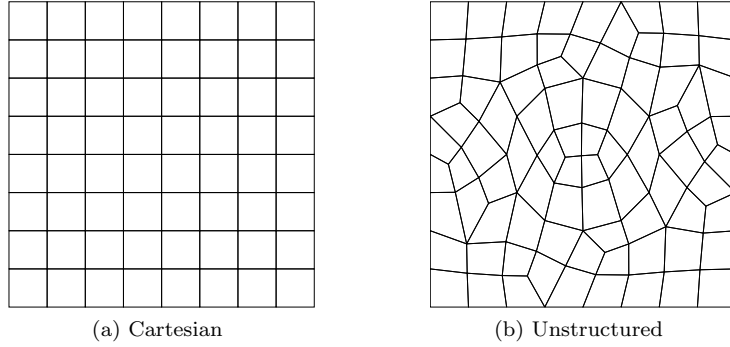


Figure 9: Base meshes for the Poisson problem. The base meshes used for $d = 3$ are the extrusion with eight layers of the two-dimensional meshes shown here.

		Cartesian						Unstructured					
		$l = 0$		$l = 1$		$l = 2$		$l = 0$		$l = 1$		$l = 2$	
p		κ	it.	κ	it.	κ	it.	κ	it.	κ	it.	κ	it.
2D	3	1.48	7	1.52	9	1.52	9	2.39	12	2.52	13	2.61	14
	7	1.48	8	1.51	9	1.51	9	3.86	17	3.74	17	3.81	17
	15	1.49	8	1.51	9	1.50	9	5.06	20	4.55	19	4.21	19
	31	1.54	9	1.53	10	1.52	10	5.66	22	4.95	21	4.48	20
3D	3	2.92	13	2.46	12	2.45	13	4.00	17	4.57	18	4.54	18
	7	2.77	13	2.69	13	2.67	13	6.50	22	6.45	22	6.29	22
	15	2.80	13	2.77	13			8.56	26	7.69	24		

Table 1: Estimated condition number and PCG iterations for the hybrid p -multigrid/Schwarz solver with the FDM/sparse relaxation. The patch problems are solved exactly on the Cartesian mesh.

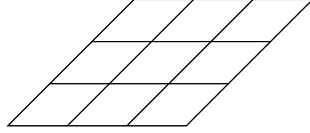


Figure 10: Parallelogram mesh used to test the spectral equivalence of the separable relaxation on a geometry where the Poisson equation is not separable. The case shown here corresponds to $\theta = 2\pi/8$.

by the square case, and the columns in Table 2b should be bounded from above by the square case. This is indeed the case, with the results in Table 2a in fact yielding better results than those guaranteed by the theory, indicating that the bound is not tight.

p	θ				
	$2\pi/4$	$2\pi/5$	$2\pi/6$	$2\pi/7$	$2\pi/8$
3	0.660	0.933	1.23	1.55	1.89
7	0.670	0.946	1.25	1.57	1.90
15	0.673	0.950	1.25	1.57	1.90

(a) Ratio $\lambda_{\min}/(1 - \cos \theta)$.

p	θ				
	$2\pi/4$	$2\pi/5$	$2\pi/6$	$2\pi/7$	$2\pi/8$
3	4.00	3.44	3.24	3.16	3.11
7	4.00	3.91	3.87	3.85	3.84
15	4.00	3.98	3.98	3.98	3.98

(b) Ratio $\lambda_{\max}/(1 + \cos \theta)$.

Table 2: Tests for the spectral equivalence of the separable relaxation on a 3×3 parallelogram mesh.

3. Primal formulation of linear elasticity

We now consider how these ideas may be applied in the more complex setting of a nonseparable, vector-valued PDE. The equations of linear elasticity describe the displacement $\mathbf{u} : \Omega \rightarrow \mathbb{R}^d$ of a solid body with a reference configuration $\Omega \subset \mathbb{R}^d$. The primal formulation is to find $\mathbf{u} - \mathbf{u}_0 \in V := [H_0^1(\Omega)]^d$ such that

$$a(\mathbf{v}, \mathbf{u}) = L(\mathbf{v}) \quad \forall \mathbf{v} \in V, \quad (3.1)$$

where

$$a(\mathbf{v}, \mathbf{u}) = \int_{\Omega} 2\mu \varepsilon(\mathbf{v}) : \varepsilon(\mathbf{u}) + \lambda \nabla \cdot \mathbf{v} \nabla \cdot \mathbf{u} \, dx, \quad L(\mathbf{v}) = \int_{\Omega} \mathbf{v} \cdot \mathbf{B} \, dx. \quad (3.2)$$

Here, we assume that the material is linear, homogeneous and isotropic, and can thus be described by the Lamé parameters $\mu, \lambda > 0$; $\varepsilon(\mathbf{u}) = (\nabla \mathbf{u} + \nabla \mathbf{u}^T)/2$ is the linearized strain tensor; \mathbf{u}_0 is Dirichlet data prescribed on the entire boundary; and $\mathbf{B} \in [L^2(\Omega)]^d$ is a body force. The Poisson ratio $\nu = \lambda/(2\mu + \lambda)$ measures the compressibility of the material. In the incompressible limit $\lambda \rightarrow \infty$ (i.e. $\nu \rightarrow 1/2$), the problem becomes ill-conditioned, as $a(\cdot, \cdot)$ becomes insensitive to divergence-free perturbations in the arguments.

Consider the partitioning of the stiffness matrix A into blocks that act on each displacement component,

$$A = \begin{bmatrix} A_{11} & \cdots & A_{1d} \\ \vdots & \ddots & \vdots \\ A_{d1} & \cdots & A_{dd} \end{bmatrix}. \quad (3.3)$$

The diagonal block A_{jj} discretizes the bilinear form

$$\int_{\Omega} \mu \nabla v_j \cdot \nabla u_j + (\mu + \lambda) \frac{\partial v_j}{\partial x_j} \frac{\partial u_j}{\partial x_j} \, d\mathbf{x}, \quad (3.4)$$

where summation is not implied, and u_j and v_j are components of \mathbf{u} and \mathbf{v} respectively. The off-diagonal blocks A_{ij} , $i \neq j$, discretize

$$\int_{\Omega} \mu \frac{\partial v_i}{\partial x_j} \frac{\partial u_j}{\partial x_i} + \lambda \frac{\partial v_i}{\partial x_i} \frac{\partial u_j}{\partial x_j} \, d\mathbf{x}. \quad (3.5)$$

The diagonal blocks can be diagonalized by the FDM on the interior of a Cartesian cell when the reference axes are aligned with the physical coordinates. The same statement does not hold true for the off-diagonal blocks, as they couple together different displacement components. This is because they discretize products of different first derivatives on the different components and hence are not separable.

The separate displacement components (SDC) preconditioner [9, 20] is defined as the block diagonal matrix $A_{\text{SDC}} = \text{diag}(A_{11}, \dots, A_{dd})$. In other words, this approach is also described as block-Jacobi in the displacement components. Our FDM-based approach can be applied on top of the SDC preconditioner, and will coincide with it on Cartesian cells aligned with the coordinate axes. On arbitrary cells, for each separate component, we obtain an auxiliary form that is separable in the reference coordinates by selecting constant diagonal coefficients $\hat{\mu}^K$. Then we obtain an auxiliary stiffness matrix $B_{\text{SDC}} = \text{diag}(B_{11}, \dots, B_{dd})$ for which the patch problems can be sparsified by the FDM, and thus cheaply solved.

It is shown in [9] that for a homogeneous isotropic material with principal axes parallel to the axes of the reference coordinate system, the condition number of the preconditioned matrix will depend on the Poisson ratio:

$$\kappa(A_{\text{SDC}}^{-1}A) \leq \frac{d-1}{\gamma} \frac{1-\nu}{1-2\nu}, \quad (3.6)$$

where γ is the constant appearing in Korn's inequality,

$$\|\mathbf{u}\|_{H^1(\Omega)^d}^2 \leq \gamma \int_{\Omega} \mathbf{u} \cdot \mathbf{u} + \varepsilon(\mathbf{u}) : \varepsilon(\mathbf{u}) \, d\mathbf{x} \quad \forall \mathbf{u} \in V. \quad (3.7)$$

Thus, the convergence rate of the SDC preconditioner will deteriorate for ν approaching 1/2, the so-called nearly incompressible case.

We consider the reference configuration $\Omega = (0, 1)^d$ discretized on a Cartesian mesh with 8 cells along each direction. We specify $\mu = 1$, a uniform downwards body force $\mathbf{B} = -0.02\mathbf{e}_2$, and homogeneous Dirichlet BCs on $\Gamma_D = \{\mathbf{x} \in \partial\Omega, x_1 = 0\}$. In Table 3 we present the PCG iteration counts required to reduce the residual by a factor of 10^8 . As the preconditioner, we employ the hybrid p -multigrid/Schwarz method with vertex-centered patches and the SDC/FDM/sparse relaxation and a coarse space with $p = 1$.

As expected from (3.6), our numerical experiments confirm that robustness with respect to ν cannot be achieved with SDC relaxation on vertex-centered patches.

		λ				
p		0	10^0	10^1	10^2	10^3
2D	3	13	14	24	70	199
	7	17	17	28	76	236
	15	18	19	30	81	249
	31	20	20	32	84	258
3D	3	20	22	39	114	362
	7	25	28	48	123	381
	15	27	29	51	125	373

Table 3: PCG iterations for the primal formulation of the linear elasticity problem using the SDC/FD-M/sparse relaxation.

4. Mixed FEM formulations of linear elasticity

In order to avoid locking in nearly incompressible continua, or impose the incompressibility constraint, the standard approach is to introduce a pressure-like variable and discretize with a mixed FEM. This is expressed by the weak formulation: find $(\mathbf{u}, p) \in V \times Q$ such that

$$a(\mathbf{v}, \mathbf{u}) + b(p, \mathbf{v}) = L(\mathbf{v}) \quad \forall \mathbf{v} \in V, \quad (4.1)$$

$$b(q, \mathbf{u}) - c(q, p) = 0 \quad \forall q \in Q. \quad (4.2)$$

where

$$a(\mathbf{v}, \mathbf{u}) = \int_{\Omega} 2\mu \varepsilon(\mathbf{v}) : \varepsilon(\mathbf{u}) \, d\mathbf{x}, \quad b(q, \mathbf{u}) = \int_{\Omega} q \operatorname{div}(\mathbf{u}) \, d\mathbf{x}, \quad c(q, p) = \int_{\Omega} \lambda^{-1} qp \, d\mathbf{x}, \quad (4.3)$$

and $Q = L_0^2(\Omega)$ for $\lambda = \infty$ and $\Gamma_D = \partial\Omega$, or $Q = L^2(\Omega)$ otherwise.

The solution for \mathbf{u} is unique if $a(\cdot, \cdot)$ is coercive on the kernel of $b(\cdot, \cdot)$, and the solution for p is unique if there exists a right inverse for $b(\cdot, \cdot)$. This is expressed in the so-called inf-sup condition or LBB condition [6, 10]: there exists β , which might depend on Ω , such that

$$0 < \beta := \inf_{q \in Q} \sup_{\mathbf{v} \in V} \frac{b(q, \mathbf{v})}{a(\mathbf{v}, \mathbf{v})^{1/2} \|q\|_Q}. \quad (4.4)$$

After selecting suitable finite dimensional subspaces $V_h \subset V$, $Q_h \subset Q$, we obtain a system of linear equations with the saddle point structure

$$\begin{bmatrix} A & B^T \\ B & -C \end{bmatrix} \begin{bmatrix} \mathbf{u} \\ p \end{bmatrix} = \begin{bmatrix} \mathbf{f} \\ g \end{bmatrix}. \quad (4.5)$$

In order for (4.5) to have a unique solution for (\mathbf{u}_h, p_h) we require the well-known Brezzi conditions: that $a(\cdot, \cdot)$ is coercive on the discrete kernel of $b(\cdot, \cdot)$, and that there exists a discrete inf-sup constant $\tilde{\beta}$ independent of the mesh but possibly depending on p such that

$$0 < \tilde{\beta} := \inf_{q_h \in Q_h} \sup_{\mathbf{v}_h \in V_h} \frac{b(q_h, \mathbf{v}_h)}{a(\mathbf{v}_h, \mathbf{v}_h)^{1/2} \|q_h\|_{Q_h}}. \quad (4.6)$$

The discretization $V_h \times Q_h$ must be chosen carefully to satisfy these conditions; they will not be satisfied by arbitrary discretizations. If they are, we have the well-known error estimates

$$\|\mathbf{u}_h - \mathbf{u}\|_V \leq C_1 \left\{ \inf_{\mathbf{v}_h \in V_h} \|\mathbf{v}_h - \mathbf{u}\|_V + \inf_{q_h \in Q_h} \|q_h - p\|_Q \right\}, \quad (4.7a)$$

$$\|p_h - p\|_Q \leq \tilde{\beta}^{-1} C_2 \left\{ \inf_{\mathbf{v}_h \in V_h} \|\mathbf{v}_h - \mathbf{u}\|_V + \inf_{q_h \in Q_h} \|q_h - p\|_Q \right\}, \quad (4.7b)$$

where $C_1, C_2 > 0$ are generic constants independent of the mesh parameter h . For the use of high-order discretizations, it is desirable to choose an element pair where $\tilde{\beta}$ does not decrease as the polynomial degree of the approximation is increased. Such a discretization is referred to as p -stable.

In fact, p -stability is important for solvers also. Approaches based on block-Gaussian elimination, such as the Uzawa algorithm [4] and block-preconditioned MINRES [31], require preconditioners for the negative pressure Schur complement $S = C + BA^{-1}B^\top$. It is well known that for the Stokes system, the continuous analogue of S , $\nabla \cdot (-\nabla^2)^{-1} \nabla$, is well approximated by the identity operator [41]. It follows that S is spectrally equivalent to the pressure mass matrix, M_p ,

$$\beta_0^2 \leq \frac{\underline{q}^\top S \underline{q}}{\underline{q}^\top M_p \underline{q}} \leq \beta_1^2 \quad \forall \underline{q} \in \mathbb{R}^{\dim(Q_h)} \setminus \{0\}. \quad (4.8)$$

The rate of convergence of block-preconditioned MINRES will be determined by the ratio β_1/β_0 . For Stokes flows with pure Dirichlet BCs, $\beta_1 = 1$, and $\beta_0 = \sqrt{d}$ otherwise. In general, we have $\beta_0 = \tilde{\beta}$. Since the top-left block A is spectrally equivalent to the vector Laplacian, these results also hold for linear elasticity. We may expect solvers based on such techniques to degrade with p -refinement if the discretization is not p -stable.

If we choose to work with the $[H^1(\Omega)]^d$ -conforming space $V_h = [Q_p(\Omega)]^d$, some standard inf-sup stable choices for Q_h are $Q_{p-1}(\Omega)$, $DQ_{p-2}(\Omega)$ and $DP_{p-1}(\Omega)$. $DQ_{p-2}(\Omega)$ denotes discontinuous piecewise polynomials of degree at most $p-2$ in each direction, while $DP_{p-1}(\Omega)$ denotes discontinuous piecewise polynomials of total degree at most $p-1$. The choice $Q_h = Q_{p-1}(\Omega)$ gives rise to the high-order generalization of the Taylor–Hood mixed element [44]. Here, M_p will not be block-diagonal, and hence more expensive preconditioning techniques will be required. Moreover, it is shown numerically in [1] that the Taylor–Hood element is not p -stable. The choice $Q_h = DQ_{p-2}$ exhibits an asymptotic decay of $\beta_h \leq Cp^{(1-d)/2}$ as $p \rightarrow \infty$ [8], and thus is not p -stable. In practice, it is observed that this is quite a pessimistic bound for moderate p [27]. The choice $Q_h = DP_{p-1}$ is p -stable, but numerical experiments reveal that the stability is severely affected by the cell aspect ratio, unlike the previous two choices [39]. Moreover this last space does not have tensor product shape functions, so its efficient implementation becomes challenging.

To construct p -stable discretizations that are also robust to cell aspect ratio, we turn to nonconforming schemes with $V_h \subset H(\text{div}, \Omega)$ [13, 23]. In particular we consider the use of Raviart–Thomas elements [3] of degree p for V_h for the displacement, paired with $Q_h = DQ_{p-1}$. This pair satisfies $\text{div}(V_h) = Q_h$, which enforces the incompressibility constraint (4.2) exactly in the numerical approximation for $\lambda = \infty$. The Raviart–Thomas elements are defined on the reference quadrilateral as

$$\text{RT}_p(\hat{K}) = P_p(\hat{\mathcal{T}}) \otimes \text{DP}_{p-1}(\hat{\mathcal{T}}) \oplus \text{DP}_{p-1}(\hat{\mathcal{T}}) \otimes P_p(\hat{\mathcal{T}}). \quad (4.9)$$

The analogous element in three dimensions is referred to as the Nédélec face element [29]. The definition can be extended to curvilinear cells via the contravariant Piola transform: for a function $\hat{\mathbf{u}} : \hat{K} \rightarrow \mathbb{R}^d$, we define $\mathbf{u} : K \rightarrow \mathbb{R}^d$ as

$$\mathbf{u} = \mathcal{P}_K(\hat{\mathbf{u}}) := \frac{1}{|DF_K|} DF_K (\hat{\mathbf{u}} \circ F_K^{-1}), \quad (4.10)$$

and set

$$\text{RT}_p(K) = \mathcal{P}_K \left(\text{RT}_p(\hat{K}) \right). \quad (4.11)$$

These elements have superb properties, but their nonconforming nature must be suitably addressed in the discretization. They only impose continuity of the normal components of \mathbf{u} across cell facets, and we therefore weakly enforce the tangential continuity via the symmetric interior penalty (SIPG) method [2]. The use of SIPG for the displacement requires further extension of the FDM/sparse relaxation; in particular, we must consider the additional facet integrals arising in the method, and show that the stiffness remains sparse.

5. Extension to interior penalty DG methods

Interior penalty discontinuous Galerkin (IP-DG) methods relax the continuity requirement of the trial space. For instance, instead of $[H^1(\Omega)]^d$, we consider a larger function space with weaker continuity, such as $[L^2(\Omega)]^d$ or $H(\text{div}, \Omega)$. As previously mentioned, in order to deal with the non-conformity, C^0 -continuity is weakly enforced via the introduction of a penalty term on the set of interior facets Γ_I of the mesh \mathcal{T}_h that vanishes for C^0 -continuous functions. Similarly, the weak prescription of the Dirichlet BC $\mathbf{u} = \mathbf{u}_0$ on Γ_D is achieved by introducing a penalty term on Γ_D .

We consider the bilinear and linear forms of the SIPG method for a purely viscous flux: $\mathcal{F}^v(\nabla \mathbf{u})$

$$\begin{aligned} a(\mathbf{v}, \mathbf{u}) &= \int_{\Omega} \nabla \mathbf{v} : \mathcal{F}^v(\nabla \mathbf{u}) \, d\mathbf{x} \\ &+ \sum_{e \in \Gamma_I \cup \Gamma_D} \int_e \eta h_e^{-1} \{G^\top\} \llbracket \mathbf{v} \rrbracket : \llbracket \mathbf{u} \rrbracket - \llbracket \mathbf{v} \rrbracket : \{\mathcal{F}^v(\nabla \mathbf{u})\} - \{G^\top \nabla \mathbf{v}\} : \llbracket \mathbf{u} \rrbracket \, ds, \end{aligned} \quad (5.1)$$

$$L(\mathbf{v}) = \int_{\Omega} \mathbf{v} \cdot \mathbf{B} \, d\mathbf{x} + \int_{\Gamma_D} \eta h_e^{-1} G^\top (\mathbf{v} \otimes \mathbf{n}) : (\mathbf{u}_0 \otimes \mathbf{n}) - G^\top \nabla \mathbf{v} : (\mathbf{u}_0 \otimes \mathbf{n}) \, ds. \quad (5.2)$$

For the vector Poisson equation, the viscous flux is given by $\mathcal{F}^v(\nabla \mathbf{u}) = \nabla \mathbf{u}$. For the primal formulation of linear elasticity, the viscous flux corresponds to the stress tensor $\mathcal{F}^v(\nabla \mathbf{u}) = \mu(\nabla \mathbf{u} + \nabla \mathbf{u}^\top) + \lambda \nabla \cdot \mathbf{u} \mathbf{1}$. For the mixed formulation of linear elasticity, the (1,1)-block of the system has viscous flux $\mathcal{F}^v(\nabla \mathbf{u}) = \mu(\nabla \mathbf{u} + \nabla \mathbf{u}^\top)$.

From left to right, the terms in the surface integral in (5.1) are referred to as the penalty, consistency, and adjoint consistency terms. The quantity G is known as the homogeneity tensor,

$$G_{ijkl} = \frac{\partial}{\partial u_{k,l}} [\mathcal{F}^v(\nabla \mathbf{u})]_{ij}, \quad (5.3)$$

for which we define the adjoint product with $\nabla \mathbf{v}$

$$[G^\top \nabla \mathbf{v}]_{kl} = G_{ijkl} v_{i,j}. \quad (5.4)$$

The average $\{\cdot\}$ and jump $[\![\cdot]\!]_e$ operators are defined for both scalar, vector, and tensor arguments as follows. Let e be a facet of the mesh. For an interior facet, let K^- and K^+ be the two mesh cells that share it, and let \mathbf{w}^- and \mathbf{w}^+ be the traces of a function \mathbf{w} on e from K^- and K^+ , respectively. On each facet we define

$$\{\mathbf{w}\}_e = \begin{cases} \frac{1}{2}(\mathbf{w}^- + \mathbf{w}^+) & e \in \Gamma_I, \\ \mathbf{w} & \text{otherwise,} \end{cases} \quad (5.5a)$$

$$[\![\mathbf{w}]\!]_e = \begin{cases} \mathbf{w}^- \otimes \mathbf{n}^- + \mathbf{w}^+ \otimes \mathbf{n}^+ & e \in \Gamma_I, \\ \mathbf{w} \otimes \mathbf{n} & \text{otherwise.} \end{cases} \quad (5.5b)$$

In order to ensure coercivity of $a(\cdot, \cdot)$ as we do h or p refinement, the penalty term must be sufficiently large. The penalty coefficient η must be chosen proportional to $(p+1)(p+d)$ [40]. On quadrilateral and hexahedral meshes, we may define the reciprocal normal length scale for an interior edge as

$$h_e^{-1} := \frac{1}{2} \left(\frac{|e|}{|K^-|} + \frac{|e|}{|K^+|} \right). \quad (5.6)$$

The stiffness matrix that corresponds to $a(\cdot, \cdot)$ in the SIPG formulation is obtained via direct stiffness summation over the cells and facets:

$$A = \sum_{K \in \mathcal{T}_h} R_K^\top A^K R_K + \sum_{e \in \Gamma_I \cup \Gamma_D} R_e^\top A^e R_e, \quad (5.7)$$

where A^K is the local submatrix discretizing the volume integral in K , R_K is the Boolean restriction onto the DOFs of K , A^e is the local submatrix discretizing the surface integral on e , and R_e is Boolean restriction onto the DOFs of the cells sharing facet e .

As an example, we consider again the scalar Poisson equation. The discrete problem is to find $u_h \in V_h = \text{DQ}_p(\Omega) \subset L^2(\Omega)$. On Cartesian cells, both A^K and A^e have a tensor product structure of the form (2.12), with matrices of operators on the interval that can be sparsified by the FDM. To illustrate this, suppose that, for $e \in \Gamma_I$, R_e reorders the DOFs such that the cells K^- and K^+ share e along the d -th reference coordinate axis, while leaving the first $d-1$ directions consistently oriented on both cells. The facet submatrices are

$$A^e = \begin{cases} E^e \otimes \hat{B} & \text{if } d = 2, \\ E^e \otimes \hat{B} \otimes \hat{B} & \text{if } d = 3, \end{cases} \quad (5.8)$$

where the interval facet matrix E^e is defined in terms of the same coefficients μ_j^K appearing in (2.12), the 1D shape functions $\{\hat{\phi}_j\}$, and their normal derivatives $\frac{\partial}{\partial n} \hat{\phi}_j$ on $\partial \hat{\mathcal{I}}$ (the usual derivative with a sign). When $e \in \Gamma_D$, $E^e \in \mathbb{R}^{(p+1) \times (p+1)}$ is given by

$$[E^e]_{ij} = \mu^e \left(\eta \hat{\phi}_i(\hat{x}^e) \hat{\phi}_j(\hat{x}^e) - \hat{\phi}_i(\hat{x}^e) \frac{\partial}{\partial n} \hat{\phi}_j(\hat{x}^e) - \frac{\partial}{\partial n} \hat{\phi}_i(\hat{x}^e) \hat{\phi}_j(\hat{x}^e) \right). \quad (5.9)$$

Here $\mu^e = \mu_l^K$, where \hat{x}_l is the reference coordinate normal to e , and $\hat{x}^e \in \partial\hat{\mathcal{I}}$ describes the facet e as the image of the plane $\hat{x}_l = \hat{x}^e$ under F_K . When $e \in \Gamma_I$, E^e is a 2×2 block matrix with blocks $E_{rs}^e \in \mathbb{R}^{(p+1) \times (p+1)}$, $r, s \in \{0, 1\}$, given by

$$[E_{rs}^e]_{ij} = \frac{(-1)^{r-s}}{2} \left(\eta(\mu_0^e + \mu_1^e) \hat{\phi}_i(\hat{x}_r^e) \hat{\phi}_j(\hat{x}_s^e) - \mu_s^e \hat{\phi}_i(\hat{x}_r^e) \frac{\partial}{\partial n} \hat{\phi}_j(\hat{x}_s^e) - \mu_r^e \frac{\partial}{\partial n} \hat{\phi}_i(\hat{x}_r^e) \hat{\phi}_j(\hat{x}_s^e) \right). \quad (5.10)$$

Here $\mu_0^e = \mu_l^{K^-}$, $\mu_1^e = \mu_m^{K^+}$, where \hat{x}_l and \hat{x}_m are the reference directions normal to e on K^- and K^+ , respectively. Similarly, the facet e is the image of $\hat{x}_l = \hat{x}_0^e$ under F_{K^-} and that of $\hat{x}_m = \hat{x}_1^e$ under F_{K^+} .

The matrices E^e are sparse in any discretization with shape functions that have an interior-interface decomposition, such as the GLL nodal functions $\{\ell_j\}$ and the hierarchical Lobatto functions $\{\hat{l}_j\}$. Since $\hat{\phi}_j(\pm 1)$ is zero except for a single value of $j \in [0, p]$, each term in (5.10) and (5.9) corresponds to a single non-zero entry, a non-zero column, and a non-zero row, as can be seen from Figure 11. Due to the interior-interface decomposition of \hat{S} , the transformed matrices $\hat{S}^\top E_{rs}^e \hat{S}$ maintain their sparsity.

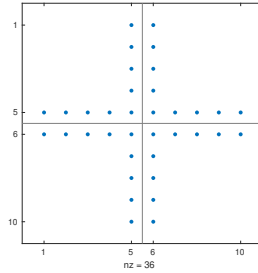


Figure 11: Non-zero structure for the interior facet matrix E^e on the interval ($p = 4$).

Most implementations of DQ_p do not feature an interior-interface decomposition and use the Gauß–Lobatto (GL) nodal shape functions which do not include the endpoints of the reference interval. This causes E^e to be no longer sparse. We can still obtain a sparse $\tilde{A} = S^\top A S$ if we use a basis with interior-interface decomposition to define transformed submatrices \tilde{A}^K, \tilde{A}^e . The transformed matrix \tilde{A} is obtained from direct stiffness summation:

$$\tilde{A} = \sum_{K \in \mathcal{T}_h} R_K^\top \tilde{A}^K R_K + \sum_{e \in \Gamma_I \cup \Gamma_D} R_e^\top \tilde{A}^e R_e. \quad (5.11)$$

We may obtain a direct inverse $A^{-1} = S \tilde{A}^{-1} S^\top$ if we interpolate the matrix of eigenvectors on an interval \hat{S} onto the GL basis without the interior-interface decomposition.

Figure 12 shows the sparsity pattern of the transformed matrix for the SIPG formulation of the Poisson equation on a Cartesian vertex-centered patch, along with its Cholesky factor. Here the matrix size is increased from $(2p-1)^d$ DOFs in the continuous case to $(2p+2)^d$. At low polynomial degrees, the interface DOFs form a large fraction of the total number, but the proportion decreases as p increases. The computational complexity analysis of Section 2.6 carries over to the discontinuous case.

This approach carries over to non-Cartesian cells for DG discretizations of the Poisson equation in the same way as the CG case. Unfortunately, the extension of our approach

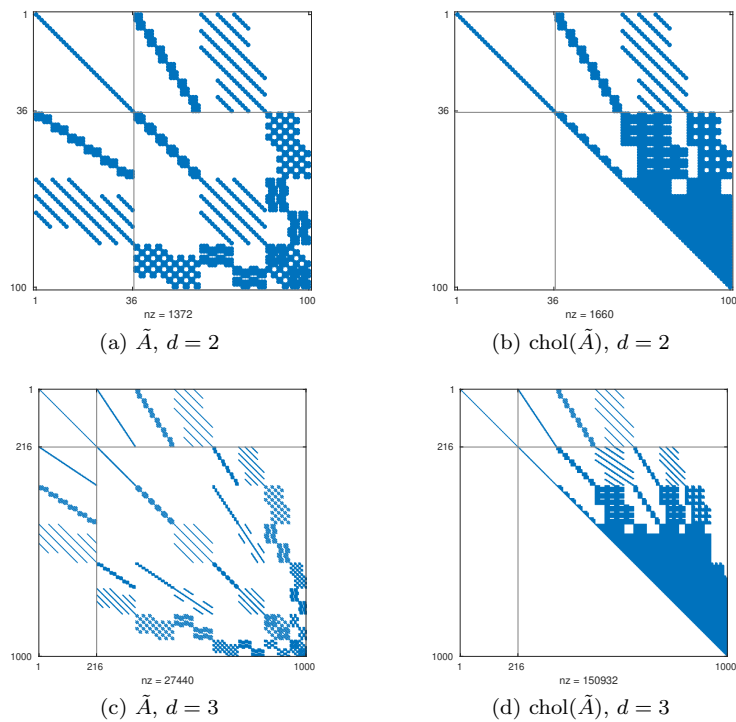


Figure 12: Non-zero structure of the SIPG stiffness matrix in the FDM basis $\tilde{A} = S^\top AS = LL^\top$ and its upper Cholesky factor L^\top for the Poisson problem on a Cartesian vertex patch with $p=4$. Since the space is discontinuous, the number of DOFs in a patch is increased. The number of non-zeros in an interior row is $3d+1$, since the interior DOFs are connected to each of the $2d$ facets of their corresponding cell, plus d more facets from the adjacent cells.

to vector-valued problems in $H(\text{div})$ on non-Cartesian cells does not yield a good preconditioner. In this setting, we construct a block-diagonal preconditioner separating the components of the DOFs, which are in the reference coordinates. For the vector Poisson problem on non-Cartesian cells, the Piola transform introduces off-diagonal contributions from the volume and surface terms, which does not occur on non-Piola-mapped elements, such as $[\mathbf{Q}_p]^d$ and $[\mathbf{DQ}_p]^d$. The excluded terms are required for the surface integral terms to vanish for arguments with C^0 continuity, and neglecting them might cause the preconditioner to become indefinite on non-Cartesian cells.

6. Results for mixed formulations of linear elasticity

We consider the same problem as in Table 3, with both a conforming $[\mathbf{Q}_p]^d \times \mathbf{DQ}_{p-2}$ discretization and a non-conforming $\text{RT}_p \times \mathbf{DQ}_{p-1}$ discretization. For the $H(\text{div})$ -conforming discretization, the normal components of the Dirichlet BCs are enforced strongly, while the tangential components of the BCs are weakly enforced with SIPG. Enforcing the normal conditions strongly is crucial for achieving a divergence-free solution in the Stokes limit $\lambda = \infty$. For the penalty coefficient, we use $\eta = (p+1)(p+d)$, which ensures a maximum eigenvalue $\beta_1 \leq 1$ for the Stokes Schur complement on a Cartesian mesh with Dirichlet BCs. We restrict our experiment to Cartesian cells, so that the FDM is applicable to the $H(\text{div})$ -conforming discretization.

We iteratively solve the discrete system (4.5) via MINRES with a symmetric positive definite block-diagonal preconditioner,

$$\mathcal{P}_{\text{diag}} = \begin{bmatrix} P_1 & 0 \\ 0 & P_2 \end{bmatrix}. \quad (6.1)$$

Here P_1 is a preconditioner for the displacement block A , and P_2 is a preconditioner for the scaled pressure mass matrix $(1 + \lambda^{-1})M_p$. For P_1 we employ the hybrid p -multigrid/Schwarz method with the SDC/FDM/sparse relaxation and a coarse space with $p = 1$ for $[\mathbf{Q}_p]^d$ and $p = 2$ for RT_p . We employ point-Jacobi on the pressure mass matrix, i.e. $P_2 = (1 + \lambda^{-1}) \text{diag}(M_p)$. When the pressure space is discretized with the GL nodal basis, and if \mathcal{T}_h consists of Cartesian cells, we have $M_p = \text{diag}(M_p)$. The solver is illustrated in Figure 13.

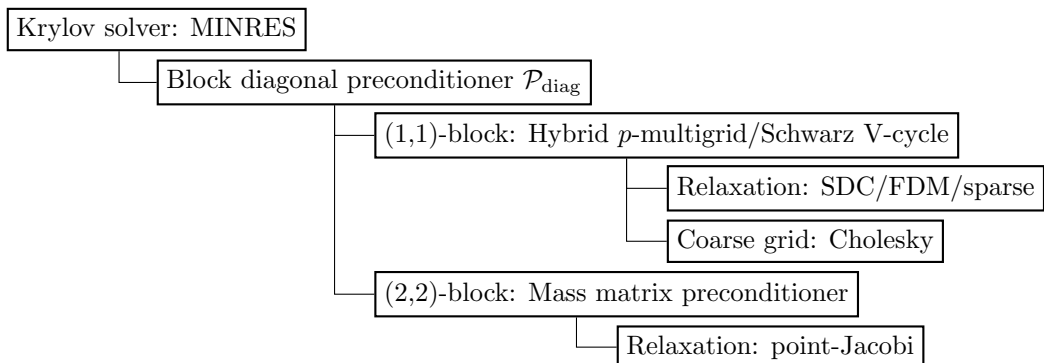


Figure 13: Solver diagram for the mixed linear elasticity problem.

In Table 4 we present MINRES iteration counts for the same configuration considered in Table 3 in Section 3, using the $[Q_p]^d \times DQ_{p-2}$ and $RT_p \times DQ_{p-1}$ elements respectively. Both discretizations yield robust iteration counts with respect to λ ; the iterations grow with the former discretization much more quickly than the latter, especially in 3D.

	p	$[Q_p]^d \times DQ_{p-2}$					$RT_p \times DQ_{p-1}$				
		λ	λ	λ	λ	λ	λ	λ	λ	λ	
		10^0	10^1	10^2	10^3	∞	10^0	10^1	10^2	10^3	∞
2D	3	28	40	43	43	43	24	38	41	42	42
	7	31	45	50	51	51	28	40	45	45	45
	15	34	50	57	57	57	30	43	48	50	50
	31	36	53	64	65	65	30	45	51	51	51
3D	3	44	67	75	76	76	34	53	60	62	62
	7	50	83	96	97	97	40	60	67	67	67
	15	53	88	111	118	118	41	63	70	71	71

Table 4: MINRES iterations for the mixed formulation of the linear elasticity problem, using the solver in Figure 13.

The solver configuration shown in Figure 13 is optimized for memory usage, employing a block-diagonal preconditioner so that the short-term recurrences of MINRES may be exploited. If one is willing to trade memory for time, one may consider an alternative configuration shown in Figure 14 employing GMRES [38] with a full block preconditioner,

$$\mathcal{P}_{\text{full}}^{-1} = \begin{bmatrix} P_1^{-1} & -P_1^{-1}B^\top \\ 0 & \mathbf{1} \end{bmatrix} \begin{bmatrix} \mathbf{1} & 0 \\ 0 & -P_2^{-1} \end{bmatrix} \begin{bmatrix} \mathbf{1} & 0 \\ -BP_1^{-1} & \mathbf{1} \end{bmatrix}, \quad (6.2)$$

which requires two applications of P_1^{-1} and a single application of P_2^{-1} per GMRES iteration. The iteration counts are presented in Table 5.

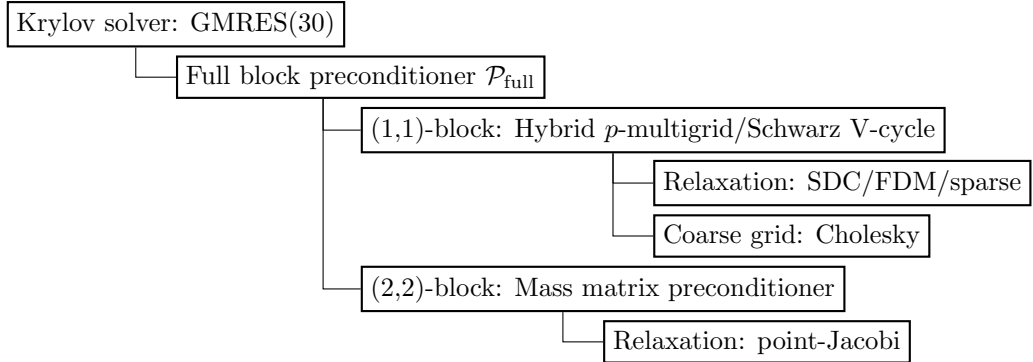


Figure 14: Solver diagram for the mixed linear elasticity problem that trades memory for iteration counts.

In Table 6 we study the performance of our solver on an unstructured mesh. We consider the $[Q_p]^d \times DQ_{p-2}$ discretization of incompressible linear elasticity ($\lambda = \infty$).

		$[Q_p]^d \times DQ_{p-2}$					$RT_p \times DQ_{p-1}$				
		λ					λ				
	p	10^0	10^1	10^2	10^3	∞	10^0	10^1	10^2	10^3	∞
2D	3	14	18	19	19	19	12	16	18	18	18
	7	16	20	22	22	22	14	17	19	19	19
	15	17	21	25	26	26	15	18	20	20	20
	31	18	22	28	29	29	16	19	21	22	22
3D	3	22	25	26	27	27	16	21	24	24	24
	7	26	29	30	30	30	19	22	24	25	25
	15	26	31	35	36	37	20	23	25	26	26

Table 5: GMRES iterations for the mixed formulation of the linear elasticity problem, using the solver in Figure 14.

We prescribe $\mu = 1$, a uniform downwards body force $\mathbf{B} = -0.02\mathbf{e}_2$, and homogeneous Dirichlet BCs on the displacement on the holes of the domain. The three-dimensional mesh is obtained via extrusion by 16 layers of the two-dimensional mesh. The iteration counts follow the same pattern as before for this element: they are not p -robust as expected, but they remain modest even at very high degrees.

	p	# DOFs	Iter.
2D	3	14 394	20
	7	76 602	24
	15	348 474	29
	31	1 482 042	35
3D	3	539 775	33
	7	12 984 039	42
	11	49 903 911	43

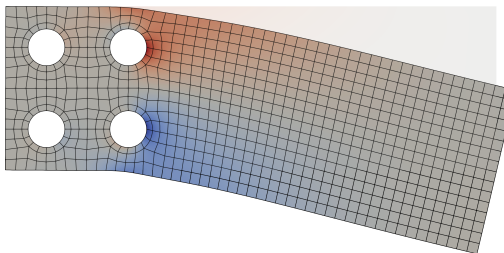


Table 6: GMRES iterations for the mixed formulation of the incompressible linear elasticity problem on the unstructured mesh shown here, using the solver in Figure 14.

7. Conclusion

We have introduced a fast relaxation method required for unstructured vertex-centered patch problems arising in Pavarino's approach, extending its practicality to much higher polynomial degrees. Our method relies on a spectrally equivalent form, constructed such that it is separable in the reference coordinates. We show promising results for the Poisson equation and mixed formulations of linear elasticity. A downside of the approach is its narrow applicability; it will not be effective on more general problems, especially for those where the dominant terms include mixed derivatives and mixed vector components. In addition, our method relies on having a good quality mesh, with its performance depending on the minimal angle; however, mesh generators with guarantees

on the minimal angle are available in two dimensions [24]. So far, we have only considered constant-coefficient problems, but the theory of [5] suggests that our approach would remain effective for spatially varying coefficients.

Acknowledgements

PDB was supported by the University of Oxford Mathematical Institute Graduate Scholarship. PEF was supported by EPSRC grants EP/V001493/1 and EP/R029423/1. We would also like to thank Lawrence Mitchell for his helpful advice for the implementation in Firedrake.

References

- [1] M. Ainsworth, P. Coggins, and B. Senior. Mixed hp -finite element methods for incompressible flow. *Chapman and Hall CRC Research Notes in Mathematics*, pages 1–20, 2000.
- [2] D. N. Arnold. An interior penalty finite element method with discontinuous elements. *SIAM J. Numer. Anal.*, 19(4):742–760, 1982.
- [3] D. N. Arnold, D. Boffi, and R. S. Falk. Quadrilateral $H(\text{div})$ finite elements. *SIAM J. Numer. Anal.*, 42(6):2429–2451, 2005.
- [4] K. J. Arrow, L. Hurwicz, and H. Uzawa. *Studies in Non-linear Programming*. Stanford University Press, 1958.
- [5] O. Axelsson and J. Karátson. Equivalent operator preconditioning for elliptic problems. *Numer. Algorithms*, 50(3):297–380, 2009.
- [6] I. Babuška. The finite element method with Lagrangian multipliers. *Numer. Math.*, 20(3):179–192, 1973.
- [7] P. D. Bello-Maldonado and P. F. Fischer. Scalable low-order finite element preconditioners for high-order spectral element Poisson solvers. *SIAM J. Sci. Comput.*, 41(5):S2–S18, 2019.
- [8] C. Bernardi, Y. Maday, and B. Métivet. Spectral approximation of the periodic-nonperiodic Navier-Stokes equations. *Numer. Math.*, 51(6):655–700, 1987.
- [9] R. Blaheta. Displacement decomposition—incomplete factorization preconditioning techniques for linear elasticity problems. *Numer. Linear Algebra Appl.*, 1(2):107–128, 1994.
- [10] F. Brezzi. On the existence, uniqueness and approximation of saddle-point problems arising from Lagrangian multipliers. *ESAIM Math. Model. Num.*, 8(R2):129–151, 1974.
- [11] C. Canuto. Stabilization of spectral methods by finite element bubble functions. *Comput. Methods Appl. Mech. Engrg.*, 116(1):13–26, 1994.
- [12] Y. Chen, T. A. Davis, W. W. Hager, and S. Rajamanickam. Algorithm 887: CHOLMOD, Supernodal Sparse Cholesky Factorization and Update/Downdate. *ACM Trans. Math. Softw.*, 35(3), 2008.
- [13] B. Cockburn, G. Kanschat, and D. Schötzau. A note on discontinuous Galerkin divergence-free solutions of the Navier–Stokes equations. *J. Sci. Comput.*, 31(1-2):61–73, 2007.
- [14] W. Couzy and M. O. Deville. A fast Schur complement method for the spectral element discretization of the incompressible Navier-Stokes equations. *J. Comp. Phys.*, 116(1):135 – 142, 1995.
- [15] L. T. Diosady and S. M. Murman. Scalable tensor-product preconditioners for high-order finite-element methods: Scalar equations. *J. Comp. Phys.*, 394:759–776, 2019.
- [16] M. Dryja and O. Widlund. *An additive variant of the Schwarz alternating method for the case of many subregions*. Technical Report 339, Ultracomputer Note 131. Department of Computer Science, Courant Institute, 1987.
- [17] P. E. Farrell, M. G. Knepley, L. Mitchell, and F. Wechsung. PCPATCH: Software for the Topological Construction of Multigrid Relaxation Methods. *ACM Trans. Math. Softw.*, 47(3), 2021.
- [18] P. F. Fischer, H. M. Tufo, and N. I. Miller. An overlapping Schwarz method for spectral element simulation of three-dimensional incompressible flows. In *Parallel Solution of Partial Differential Equations*, pages 159–180. Springer, 2000.
- [19] A. George. Nested dissection of a regular finite element mesh. *SIAM J. Numer. Anal.*, 10(2):345–363, 1973.

- [20] I. Gustafsson and G. Lindskog. On parallel solution of linear elasticity problems: Part I: theory. *Numerical Linear Algebra with Applications*, 5(2):123–139, 1998.
- [21] G. Karniadakis and S. Sherwin. *Spectral/hp element methods for computational fluid dynamics*. Oxford University Press, 2013.
- [22] C. Lanczos. An iteration method for the solution of the eigenvalue problem of linear differential and integral operators. 1950.
- [23] P. L. Lederer and J. Schöberl. Polynomial robust stability analysis for $H(\text{div})$ -conforming finite elements for the Stokes equations. *IMA J. Numer. Anal.*, 38(4):1832–1860, 2018.
- [24] X. Liang and Y. Zhang. Hexagon-based all-quadrilateral mesh generation with guaranteed angle bounds. *Comput. Methods Appl. Mech. Engrg.*, 200(23):2005–2020, 2011.
- [25] J. W. Lottes and P. F. Fischer. Hybrid multigrid/Schwarz algorithms for the spectral element method. *J. Sci. Comput.*, 24(1):45–78, 2005.
- [26] R. E. Lynch, J. R. Rice, and D. H. Thomas. Direct solution of partial difference equations by tensor product methods. *Numer. Math.*, 6:185–199, 1964.
- [27] Y. Maday, D. Meiron, A. T. Patera, and E. M. Rønquist. Analysis of iterative methods for the steady and unsteady Stokes problem: Application to spectral element discretizations. *SIAM J. Sci. Comput.*, 14(2):310–337, 1993.
- [28] J.-F. Maitre and O. Pourquier. Condition number and diagonal preconditioning: comparison of the p -version and the spectral element methods. *Numer. Math.*, 74(1):69–84, 1996.
- [29] J.-C. Nédélec. Mixed finite elements in \mathbb{R}^3 . *Numer. Math.*, 35(3):315–341, 1980.
- [30] S. A. Orszag. Spectral methods for problems in complex geometries. *J. Comp. Phys.*, 37(1):70–92, 1980.
- [31] C. C. Paige and M. A. Saunders. Solution of sparse indefinite systems of linear equations. *SIAM J. Numer. Anal.*, 12(4):617–629, 1975.
- [32] L. F. Pavarino. Additive Schwarz methods for the p -version finite element method. *Numer. Math.*, 66(1):493–515, 1993.
- [33] L. F. Pavarino, E. Zampieri, R. Pasquetti, and F. Rapetti. Overlapping Schwarz methods for Fekete and Gauss–Lobatto spectral elements. 29(3):1073–1092, 2007.
- [34] W. Pazner. Efficient low-order refined preconditioners for high-order matrix-free continuous and discontinuous Galerkin methods. *SIAM J. Sci. Comput.*, 42(5):A3055–A3083, 2020.
- [35] W. Pazner and P.-O. Persson. Approximate tensor-product preconditioners for very high order discontinuous Galerkin methods. *J. Comp. Phys.*, 354:344–369, 2018.
- [36] W. Pazner and P.-O. Persson. Interior penalty tensor-product preconditioners for high-order discontinuous Galerkin discretizations. In *2018 AIAA Aerospace Sciences Meeting*, page 1093, 2018.
- [37] J.-F. Remacle, R. Gandham, and T. Warburton. GPU accelerated spectral finite elements on all-hex meshes. *J. Comp. Phys.*, 324:246–257, 2016.
- [38] Y. Saad and M. H. Schultz. GMRES: a generalized minimal residual algorithm for solving nonsymmetric linear systems. *SIAM J. Sci. Stat. Comput.*, 7(3):856–869, 1986.
- [39] D. Schötzau and C. Schwab. Mixed hp -FEM on anisotropic meshes. *Math. Models Methods Appl. Sci.*, 8(05):787–820, 1998.
- [40] K. Shahbazi. An explicit expression for the penalty parameter of the interior penalty method. *J. Comp. Phys.*, 205(2):401–407, 2005.
- [41] D. Silvester and A. Wathen. Fast iterative solution of stabilised Stokes systems Part II: using general block preconditioners. *SIAM J. Numer. Anal.*, 31(5):1352–1367, 1994.
- [42] J. Stiller. Robust multigrid for Cartesian interior penalty DG formulations of the Poisson equation in 3D. In M. L. Bittencourt, N. A. Dumont, and J. S. Hesthaven, editors, *Spectral and High Order Methods for Partial Differential Equations ICOSAHOM 2016*, pages 189–201, Cham, 2017. Springer International Publishing.
- [43] B. Szabó and I. Babuška. *Finite element analysis*. John Wiley & Sons, 1991.
- [44] C. Taylor and P. Hood. A numerical solution of the Navier-Stokes equations using the finite element technique. *Comput. Fluids*, 1(1):73–100, 1973.
- [45] J. Witte, D. Arndt, and G. Kanschat. Fast tensor product Schwarz smoothers for high-order discontinuous Galerkin methods. *J. Comput. Methods Appl. Math.*, 2020.
- [46] J. Xu. The auxiliary space method and optimal multigrid preconditioning techniques for unstructured grids. *Computing*, 56(3):215–235, 1996.